PAPER

Effect of polydiacetylene-based nanosomes on cell viability and endocytosis

IOP Publishing Nanotechnology
Nanotechnology 30 (2019) 245101 (10pp) https://doi.org/10.1088/1361-6528/ab0ccf

Effect of polydiacetylene-based nanosomes on cell viability and endocytosis

Kyu Ha Park[1,2,7], Minhee Ku[3,4,5,7], Nara Yoon[3,4,5], Dae Youn Hwang[1,2], Jaebeom Lee[6], Jaemoon Yang[3,4,5,8] and Sungbaek Seo[1,2,8]

[1] Department of Biomaterials Science, Pusan National University, Miryang 50463, Republic of Korea
[2] Life and Industry Convergence Institute, Pusan National University, Miryang 50463, Republic of Korea
[3] Department of Radiology, College of Medicine, Seoul 03722, Republic of Korea
[4] Systems Molecular Radiology, Yonsei University, Seoul 03722, Republic of Korea
[5] Research Institute of Radiological Science, Yonsei University, Seoul 03722, Republic of Korea
[6] Department of Chemistry, Chungnam National University, Daejeon 34134, Republic of Korea

E-mail: 177HUM@yuhs.ac and sbseo81@pusan.ac.kr

Received 11 December 2018, revised 5 February 2019
Accepted for publication 5 March 2019
Published 1 April 2019

Abstract

Polydiacetylene-based nanoparticles have been developed as nanocarriers for various bio-applications. However, how nanocarriers enter the cell environment and affect cell viability has not yet been considerably explored. In this study, polydiacetylene-based nanoliposomes (nanosomes) were electrostatically complexed with rhodamine fluorophores. Based on real-time cell imaging and cell viability assessment, the most highly polymerized nanosomes were found to be less toxic to cells. Moreover, it was revealed that the rhodamine/polydiacetylene nanosome complex dissociates at cell environment, the polydiacetylene nanosome penetrates into cells, as suggested by the fluorescence observed in confocal microscopy images.

Supplementary material for this article is available online

Keywords: nanosome, electrostatic complex, cell viability, endocytosis

(Some figures may appear in colour only in the online journal)

1. Introduction

Nanoparticles have been widely studied for their potential use as biocompatible carriers, owing to their benefits such as controlled loading capacity, multi-functionality, and improved circulation time [1]. Several material-based nanoparticles have been considered for use as delivery vesicles, sensing platforms, or imaging probes [2–7]. The cell viability and cellular uptake of these nanocarriers were usually evaluated by the MTT assay and confocal microscopic imaging or live cell imaging.

Polydiacetylene (PDA) is an attractive material that can change color and emit fluorescence due to external stimuli such as temperature [8, 9], pH [10, 11], mechanical stress [12, 13], and binding interactions [14–16]. Receptor-ligand interactions can stimulate the optical transition of PDA from blue to red or induce it to emit red fluorescence. With this optical transition, PDA can provide information regarding binding events or spatial information on where it is transported due to the interaction.

PDA-based nanoparticles have been utilized for various bio-applications, including their use as drug delivery carriers [17–19], for chemo/biosensing platforms [16, 20, 21], and as imaging probes [22, 23]. The Doris group has established PDA-based delivery micelles using the supramolecular self-assembly of diacetylene-containing amphiphiles [17, 19, 23]. They systematically investigated the *in vivo* tumor targeting efficiency of the micelles in drug delivery and tumor imaging. The Schmuck group synthesized peptides containing diacetylene, which self-assembled into varied nanostructures that could be used as cell imaging probes [22]. Interestingly, concentration-dependent self-assembled peptides such as

[7] KHP and MK contributed equally to this work. The manuscript was written through the contributions of all authors. All authors have given approval to the final version of the manuscript.
[8] Authors to whom any correspondence should be addressed.

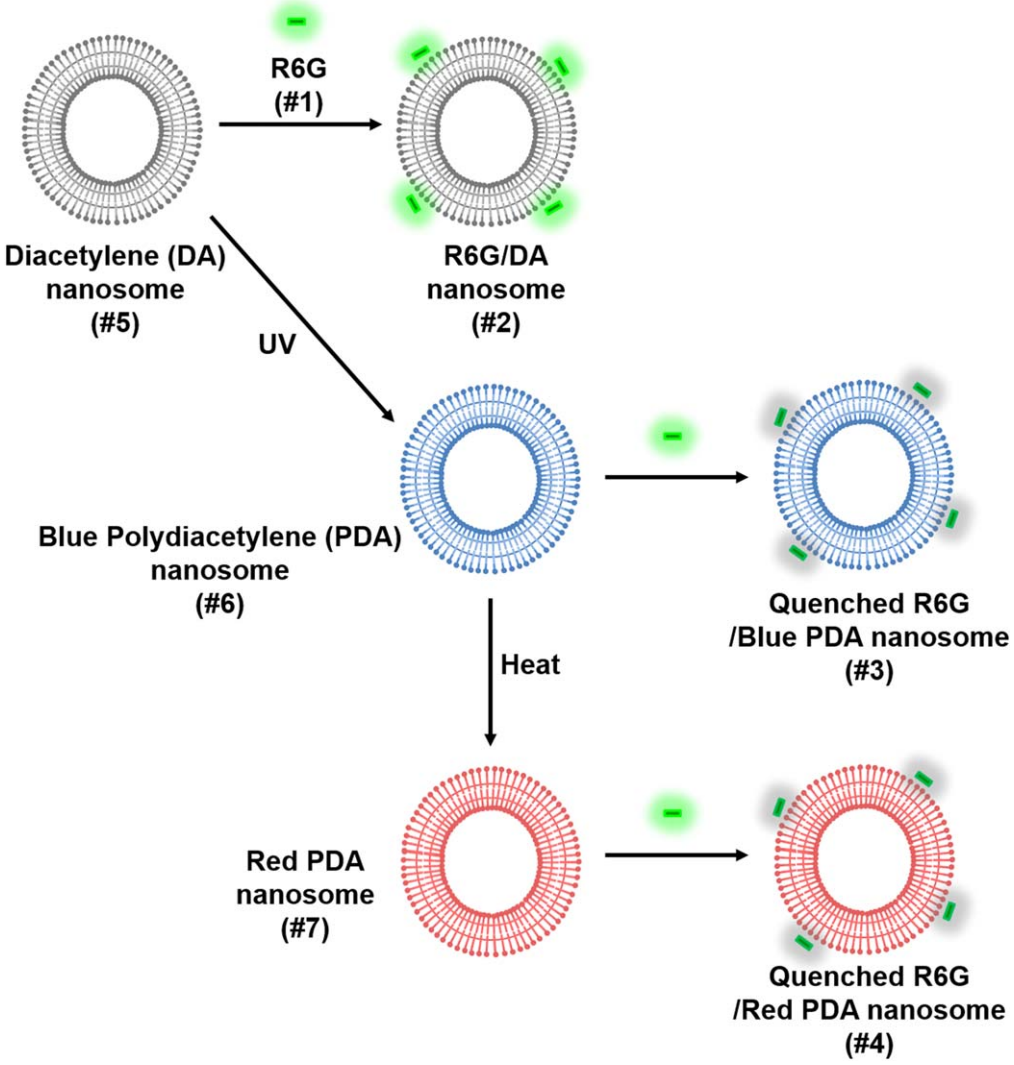

Figure 1. Schematic illustration for the preparation of PDA-based nanosomes and their fluorescent labeling.

vesicles and tadpole- and bola-shaped assemblies can translocate into HeLa cells; however, nanofiber-like assemblies surround the cell membranes. Since time-consuming steps are required for the synthesis of amphiphiles, we are interested in developing PDA-based nanoliposomes (nanosomes) entirely consisting of the commercial and commonly used diacetylene [10,12-pentacosadiynoic acid (PCDA)] monomer, for use as versatile nanocarriers. To our knowledge, how this PDA-based nanocarrier interacts with cells and influences cell viability and endocytosis has not yet been fully explored.

In this work, several PDA-based nanosomes were prepared to study their effect on cell viability, as well as observe the routes they take to move towards cells (figure 1). The application of PDA nanosomes as sensing platforms and as imaging probes is limited due to the low red fluorescence quantum yield of the PDA molecules (~0.02%) [24, 25]. Therefore, rhodamine 6 G (R6G) was electrostatically complexed with the diacetylene (DA) nanosomes to serve as a secondary tracking fluorophore. *In vitro* cell imaging by real-time microscopic images and the MTT assay were performed to track the movement of the nanosomes towards the cell environment and effect on cell viability.

2. Experimental details

2.1. Materials and methods

All solvents were purchased from DAEJUNG Chemicals, Korea. 10,12-Pentacosadiynoic acid (PCDA) was purchased from Alfa Aesar, USA. Rhodamine 6 G was purchased from Tokyo Chemical Industry, Japan. Dialysis membrane (Cellu·Sep®, MWCO = 3500 Da) was purchased from Membrane Filtration Products, Inc., USA.

The morphology of the PCDA assembly structures was observed through transmission electron microscopy (TEM) using H-7500 system (Hitachi) operating at 80 kV. The size distribution and zeta potential of the liposome solutions were measured using a Zetasizer Nano ZS90 (Malvern Instruments). A handheld UV lamp (254 nm, 1 mW cm^{-2}) was applied for the photopolymerization of PCDA nanosomes.

2.2. Preparation of PDA-based nanosomes

Diacetylene nanoliposome (DA nanosome) solutions were prepared using the injection method described in a previous study [26]. PCDA Powder (3.75 mg) was dissolved in acetone (300 μl) and injected into deionized (DI) water (20 ml) (i.e. DA nanosome, #5) and 0.008 33 mM Rhodamine 6 G solution (20 ml) (i.e. R6G/DA nanosome, #2), to yield a final PCDA concentration of 0.5 mM in the nanosomes. The samples were filtered through a syringe filter cellulose acetate membrane with a pore size of 0.8 μm and stored at 4 °C for at least 4 h. Then, the DA nanosomes (#5) were irradiated with UV (254 nm) for 1, 3, 5, 8, and 10 min (Blue PDA nanosome, #6), and half volumes of each sample were heated at 80 °C (Red PDA nanosome, #7). The samples were centrifuged at 12 000 rpm for 20 min at 4 °C and separated from the supernatant. To the Blue PDA and Red PDA nanosome solutions (10 ml each), 0.008 33 mM R6G solution (10 ml) was added to make R6G/Blue PDA nanosome (#3) and R6G/Red PDA nanosome (#4), respectively.

2.3. UV–vis absorption and photoluminescence measurements of PDA-based nanosomes

The UV–vis absorption spectra of the nanosome solutions (200 μl in 96-well plates) were obtained using the Biotek Spectrophotometer (Epoch). The fluorescence emission spectra of the nanosome solutions were measured using the fluorescence spectrophotometer F-7000 (Hitachi). R6G (#1), R6G/DA nanosome (#2), R6G/Blue PDA nanosome (#3), and R6G/Red PDA nanosome (#4) solutions were diluted by 3/20 (0.001 25 mM R6G) to limit the photoluminescence (PL) intensity ($y < 10\,000$). The excitation wavelength was set at 480 nm and the fluorescence emission spectra were observed at 500–700 nm.

2.4. Real-time cell imaging

MDA-MB-231 cells (1×10^5 cells/well) were cultured in a 24-well plate in Roswell Park Memorial Institute 1640 (RPMI 1640; Gibco) growth medium supplemented with 10% fetal bovine serum (FBS) and 1% antibiotic-antimycotic supplemented at 37 °C, 5% CO_2. After incubation for 24 h, the medium was aspirated out of the plate and replaced with phosphate-buffered saline (PBS, control; #0), R6G only (#1), or nanosome solutions (#2–#8) in phenol red-free medium. The cells were monitored at 10 min intervals for 24 h using the Live Cell Imaging System (DMI6000B) with a 20×objective lens, and the data were processed using the LAS X software (ver. 1,1,12 420,0, Leica Microsystems CMS GmbH).

2.5. Cell viability evaluation by crystal violet staining and MTT assay

To measure the cell cytotoxicity of the nanosomes, the viable adherent cell population was measured through the crystal violet (CV) assay. After real-time cell imaging, the media containing the nanosome solutions were removed and the cells were fixed with 4% paraformaldehyde (Biosesang) for 15 min. Cells were stained with crystal violet solution (50 ml of 1% crystal violet solution, 25 ml of distilled H_2O, and 25 ml of methanol; Sigma) and were quantified using ImageJ. Cell viability was evaluated using 3-(4,5-dimethylthiazoly-2)-2,5-diphenyltetrazolium bromide (MTT; Sigma) based on the cellular reduction. MDA-MB-231 cells were seeded in 96-well plates at a density of 1×10^4 cells/well. After incubation for 48 h, R6G only (#1) or nanosome solutions (#2–#8) in phenol red-free medium was added to cells and incubated for 4 and 24 h. The cells were then incubated for 4 h at 37 °C with MTT reagent. MTT solvent (10% SDS in 0.01 M HCl) was added to each well to solubilize the insoluble formazan product overnight. The optical density (OD) was measured at 584 nm and 650 nm as a control using a microplate reader (Cytation 1, BioTek Instruments). Data are shown as the average ± the standard deviation ($n = 4$).

2.6. Fluorescence and confocal microscopic imaging of cells

MDA-MB-231 cells were plated on a 24-well plate (for fluorescence imaging) and on round-shape glass coverslips in a 4-well plate (for confocal microscopic imaging) at a density of 1×10^5 cells/well. After 24 h of incubation, the cells were treated with the nanosome solutions (#1–#8) for another 24 h. The fluorescence signals of rhodamine 6 G (R6G) were measured using an excitation filter at 500–550 nm and emission filter at 590–650 nm with DMI6000B using a 10×objective lens and the LAS X software. To investigate the intracellular trafficking of nanosomes, cells were fixed for 30 min with 4% paraformaldehyde (Biosesang), washed three times with 1×PBS (WELGENE), and permeabilized with 0.5% Triton X-100 for 15 min. The cells were washed and blocked with 0.1% bovine serum albumin (BSA; Amresco) and 0.001% sodium azide (JUNSEI Chemical) in PBS. To visualize the subcellular colocalization of the nanosomes with the early endosomes, the cells were stained with rabbit anti-early endosome antigen 1 protein (EEA1) polyclonal antibody (Abcam) and either goat anti-rabbit IgG (H&L) DyLight™ 350-conjugated antibody (Thermo Scientific) or Alexa Fluor® 594-conjugated antibody (Abcam). A nuclear staining solution with Hoechst 33 342 (Molecular Probes) was added at a final concentration of 5 mg ml^{-1}. Images were obtained using a confocal microscope (LSM-700, Carl Zeiss, Jena, Germany) with a 63×objective using the ZEN software (version 5.5.0.375, Carl Zeiss). Excitation filters were set at 332 (DyLight 350) and 590 (Alexa Fluor 594) nm for EEA1 and 497 nm for R6G fluorescent signals, respectively.

2.7. Statistical analysis

All data of the cell viability results in this article are presented as the mean ± standard deviation. Student's *t*-test was used to confirm the significance of the comparison. *P* values of less than 0.05 were considered to statistically significant.

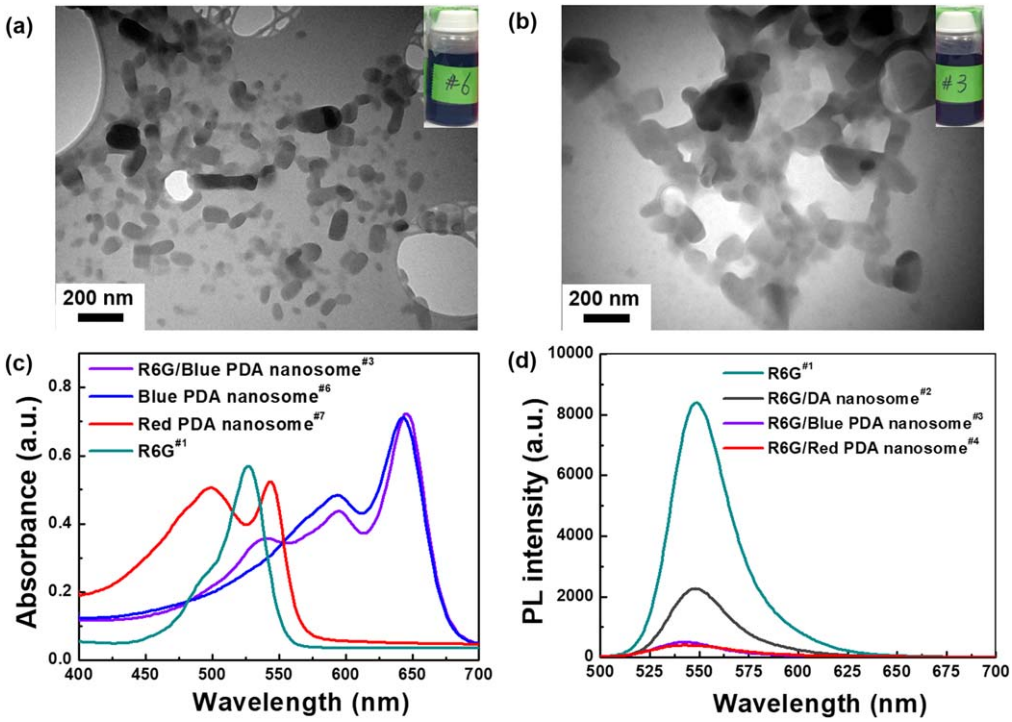

Figure 2. TEM image of (a) Blue PDA nanosome (#6) and (b) R6G/Blue PDA nanosome (#3). Inset: photos of the suspended nanosomes. Scale bars of the images are 200 nm. (c) UV–vis absorption spectra of the nanosomes (#1, #3, #6, and #7). (d) PL spectra of the nanosomes (#1, #2, #3, and #4) at $\lambda_{ex} = 480$ nm.

3. Results and discussion

PDA-based nanosomes can carry fluorophores such as R6G on their surfaces by electrostatic complexation [27]. In the previous study, we observed quenching of R6G at the surface of nanosomes by forming R6G H-aggregates and, conversely, recovering R6G emission when R6G is dissociated from the surface of the nanosomes. Herein, we were interested in monitoring nanosomes (figure S1 is available online at stacks.iop.org/NANO/30/245101/mmedia) by tracking two fluorophores (PDA in red form and R6G). The fundamental understanding of how nanosomes behave when moving toward cell environments and where the two fluorophores (PDA and R6G) localize in a single platform can provide insights that may aid the design of PDA-based nanocarriers for *in vitro* study and further translational research.

A DA nanosome (#5) consisting of a PCDA amphiphile monomer was prepared as a primary platform by forming a self-assembled structure in an aqueous environment. Due to the low quantum yield of PDA, R6G as a secondary tracking marker was complexed with a PDA nanosome to make the R6G/Blue PDA nanosome (#3). As sensing materials and imaging probes, the quenching of R6G at the surface of the Blue PDA nanosome (#6) is interesting to observe how the nanosome interacts with cells, as well as whether if the PDA will undergo optical transition upon interaction with cells.

The Blue PDA nanosome (#6) assembled into spherical formations that were 50–120 nm in diameter as observed through TEM (figure 2(a)). After electrostatic complexation with R6G, the R6G/Blue PDA nanosome (#3) maintained sphere-shaped with a slight larger size of 100–150 nm in diameter (figure 2(b)). The light scattering measurements revealed that the sizes of the Blue PDA nanosome (#6, 165 ± 77 nm) and R6G/Blue nanosome (#3, 158 ± 81 nm) were consistent (figure S2). The zeta potential of the Blue PDA nanosome and the R6G/Blue PDA nanosome were −45 ± 6 mV and −31 ± 6 mV, respectively. These findings indicate that R6G was bound on surface of the Blue PDA nanosome, while it retained a similar size as the original nanosome.

The R6G/Blue PDA nanosome (#3) showed the characteristic UV–vis absorption spectra of the PDA backbone ($\lambda_{max} = 646$ nm, blue color) and R6G ($\lambda_{max} = 540$ nm), indicating the presence of PDA and R6G together in a single platform (figure 2(c)). The shift of wavelength of maximum absorption ($\lambda_{max} = 526$ nm) of R6G implies interactions of the electrostatic complexation. After 1 d of dialysis (removal process of weakly bound R6G on surface of PDA nanosome), the purified nanosome maintained the characteristic UV–vis absorption spectra of PDA and R6G (figure S3).

After electrostatic complexation, the emission of R6G (mainly in the range of 525–600 nm) was quenched or reduced with nanosomes #2, #3, and #4 by 73.1, 94.1, and 95.3%, respectively (figure 2(d)). The quenching of R6G in R6G/DA nanosome (#2) can be attributed to the self-assembled H-type aggregates of cationic R6G that formed on the surface of negatively charged DA nanosomes [27]. The fluorescence of R6G in R6G/Blue PDA nanosome (#3) and R6G/Red PDA nanosomes (#4) was dramatically quenched by the fluorescence resonance energy transfer from R6G to the PDA-conjugated backbone [28–30]. The similar quenching efficiencies of R6G in the R6G/Blue PDA nanosome

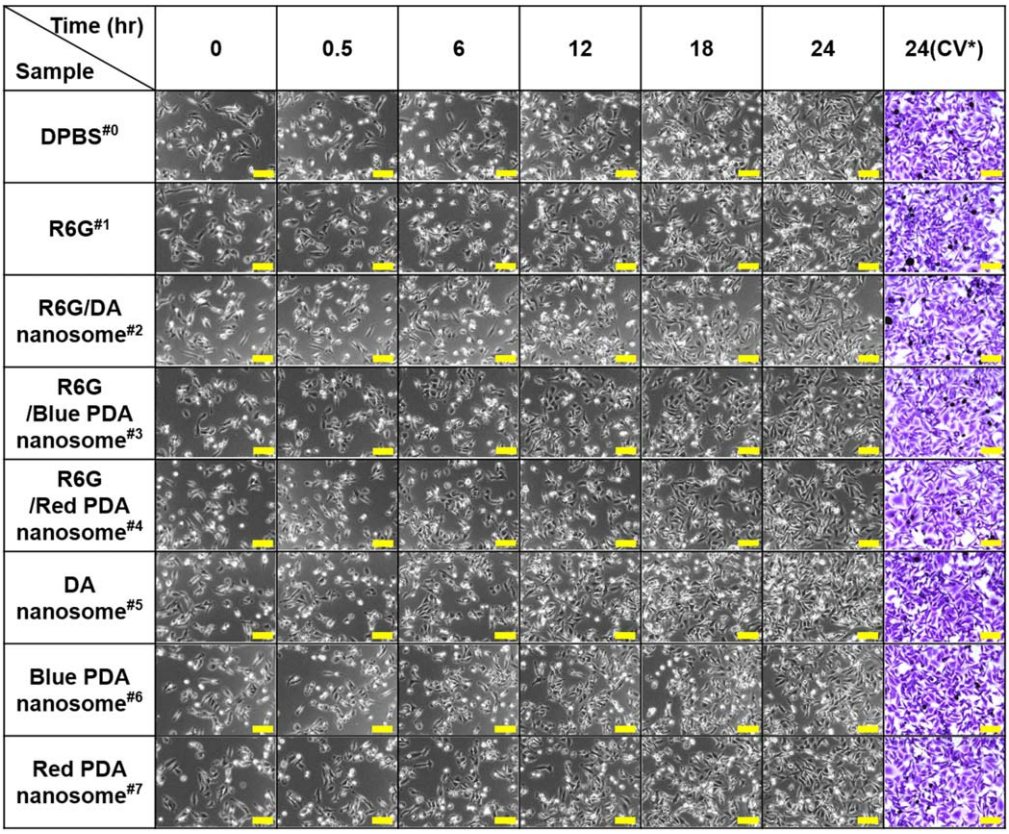

Figure 3. Microscopic images of MDA-MB-231 cells incubated with nanosomes (#1–#7) obtained using a 20×objective lens at each time point. The time-points (in hours) we have described represent the time periods for which the cells were incubated after treatment with the nanosomes. The images of cells treated with R6G (0.000 833 mM) or/and PCDA (0.05 mM)—1/10 dilution of the stock solutions of R6G (0.008 33 mM) or/and PCDA (0.5 mM), and incubated for each time point, i.e. 0, 0.5, 6, 12, 18, and 24 h. *CV: Crystal violet staining. Scale bars of the microscopic images represent 100 μm.

(#3, 94.1%) and in the R6G/Red PDA nanosome (#4, 95.3%) may be attributed to the similar energy transfer efficiency from the broad UV–vis absorption (400–600 nm) of the Blue PDA nanosome and the Red PDA nanosome, as shown in figure 2(c).

As a potential nanocarrier, PDA-based nanosomes consisting of solely PCDA diacetylene are advantageous due to their simple preparation requirements and good colloidal stability; however, they have not been fully explored in terms of their effect on cell viability and their interaction with cells. In order to observe changes in cell morphology and in the density of cell growth upon adding the nanosomes, the MDA-MB-231 cells were monitored for 24 h. We seeded MDA-MB-231 cells in a 24-well plate at a density of 1×10^5 cells/well, and incubated the cells for 24 h. For time-lapse imaging, the cells were stably attached to the bottom of the well plate; then, the growth medium was removed and replaced with the sample solutions (#0–#7). The cells were monitored at 10 min intervals for 24 h using the Live Cell Imaging System. In all the cases (DPBS as control and #1–#7), cells maintained their normal morphology and growth rate (figure 3). After 24 h of incubation, cells were stained with crystal violet to count number of live cells. The cells remained viable regardless of the introduced nanosomes (figure S4).

To investigate effect of the nanosomes on cell viability, MTT assay was performed at 4 and 24 h. It was noted that the blue color of the R6G/Blue PDA nanosome (#3) and the Blue PDA nanosome (#6) became reddish upon mixing preheated (37 °C) cell culture medium. We continued following the experiments to check if any different effect on cell viability between samples (#3, #6) of becoming red colored during the mixing process and samples (#4, #7) of purposely prepared red colored. At 4 h of treatment, cell viability decreased as the concentration of the nanosome treatment increased (figure 4(a)).

After 24 h of incubation with the nanosomes, R6G alone (#1) was found to be less toxic to cells than the nanosomes containing DA or PDA (#2–#4) (figure 4(b)). Moreover, the nanosomes containing a higher degree of polymerization were found to be less toxic to cells than non-polymerized nanosomes (#3, #4 relative to #2; #6, #7 relative to #5), especially for dilutions greater than 0.01. This may be attributed to the greater toxicity of DA monomers compared to that of polymers (e.g. PDA). Accordingly, PDA-based nanocarriers are advantageous due to their lower levels of toxicity compared to non-polymerized DA-based nanocarriers, in addition to their benefits of colloidal stability and drug loading efficiency [31].

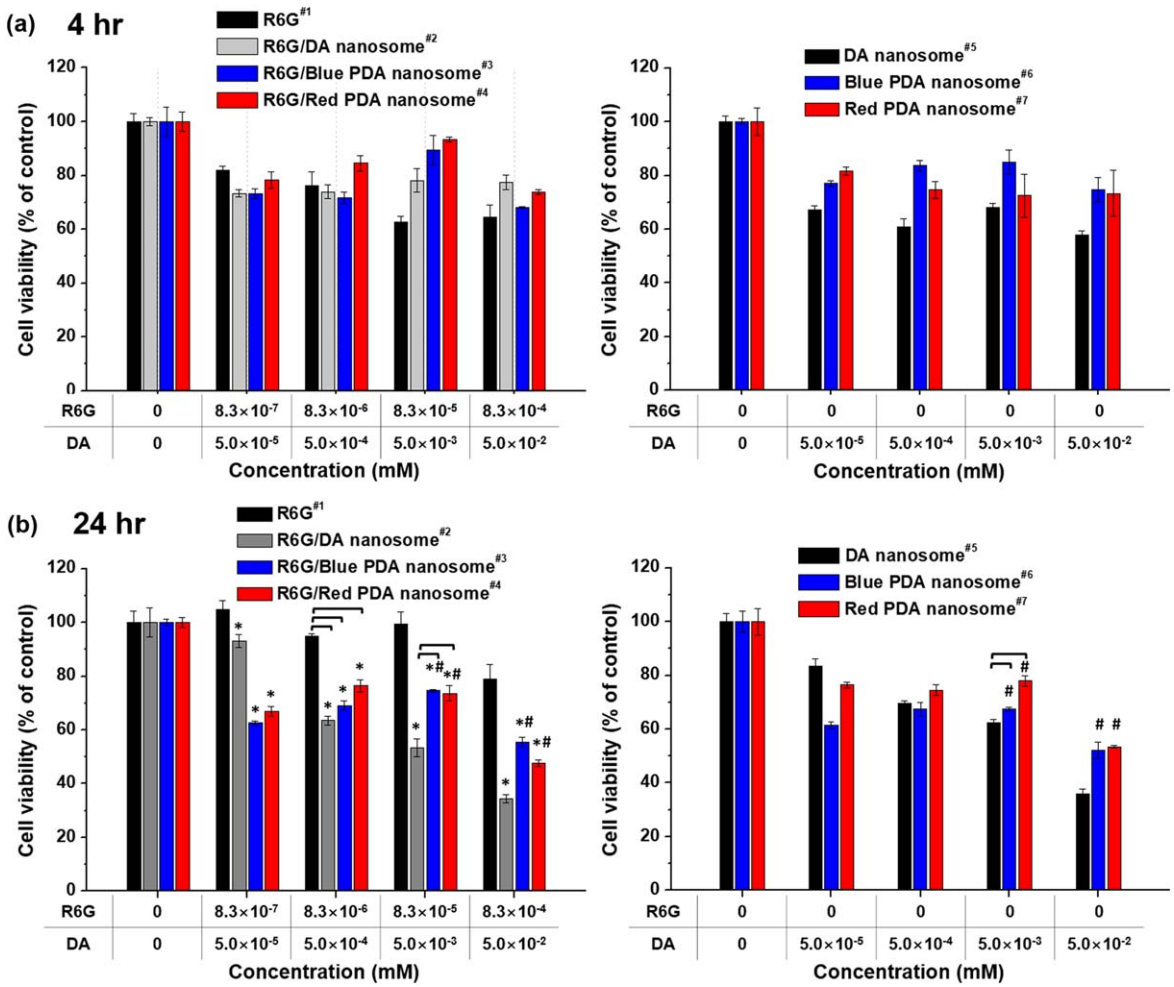

Figure 4. Effect of nanosomes (#1–#7) on cell viability evaluated by MTT assay. MDA-MB-231 cells were treated with nanosomes in PBS solution (1/10 serial dilution of stock* consisting of R6G (0.008 33 mM) or/and PCDA (0.5 mM)). (a) 4 h and (b) 24 h of treatment with each nanosome solution. Data are means ± standard deviation.*, $P < 0.05$ relative to R6G$^{\#1}$ group. #, $P < 0.05$ relative to DA-containing nanosome$^{\#2/\#5}$ group.

Blue PDA nanosomes that were irradiated with UV longer (i.e. more photopolymerized) showed less toxicity to cells than those irradiated with UV for shorter periods (figure S5). This also supports the point that the existence of non-polymerized molecules (i.e. DA monomers) considerably affected to cellular viability.

To investigate the behavior of the nanosomes with regards to their movement towards cells and uptake pathway, epi-fluorescence microscopy (FM) and confocal fluorescence microscopy (CFM) images of the cells were performed. While using epi-fluorescence microscopy, it is difficult to distinguish the accurate site of fluorescent molecules. In figure 5(a), we could observe the red fluorescence signals (λex = 500–550 nm and λem = 590–630 nm) in the presence of R6G without a rinsing process. However, after washing the incubated cells with PBS, the fluorescence signals were not detected in the epi-fluorescence microscopy analysis at all experimental conditions. We thus performed z-stacked confocal microscopy (figure 5(b), fourth column) analysis of the nanosome-treated cells to investigate the position of the fluorescent nanosomes after the incubated cells were washed with PBS. As presented in figure 5(b), the blue spots from EEA1 (endosome marker, $\lambda_{ex} = 332$ nm, $\lambda_{em} = 435$ nm) were distributed at the cytosol. The dark circular region due to a nucleus was observed in the confocal microscopy images. Moreover, red spots ($\lambda_{ex} = 497$ nm, $\lambda_{em} = 524$ nm) from PDA-nanosomes were also visualized at the cytosol. No red fluorescent signals were detected at the membrane and nucleus for all experimental conditions. In figures 5(a) and (b), R6G (#1) treatment showed red fluorescence near cells as observed in the FM image at filter 530 (λ_{ex} = 500–550 nm, λ_{em} = 590–650 nm) and the CFM images. This suggests that R6G did not penetrate into the cells and simply coated the cells externally. On the contrary, the Blue PDA nanosome (#6) and the Red PDA nanosome (#7) did not show red fluorescence in the FM images at filter 530, while vivid red fluorescence was observed in the CFM image at filter 435 nm and FM spectra (figure S6), indicating that the PDA nanosomes were internalized by the cells. In order to support the co-localization of the CFM images, we quantified the fluorescent intensities at each wavelength of emission (λem = 435 and λem = 524) from the obtained confocal

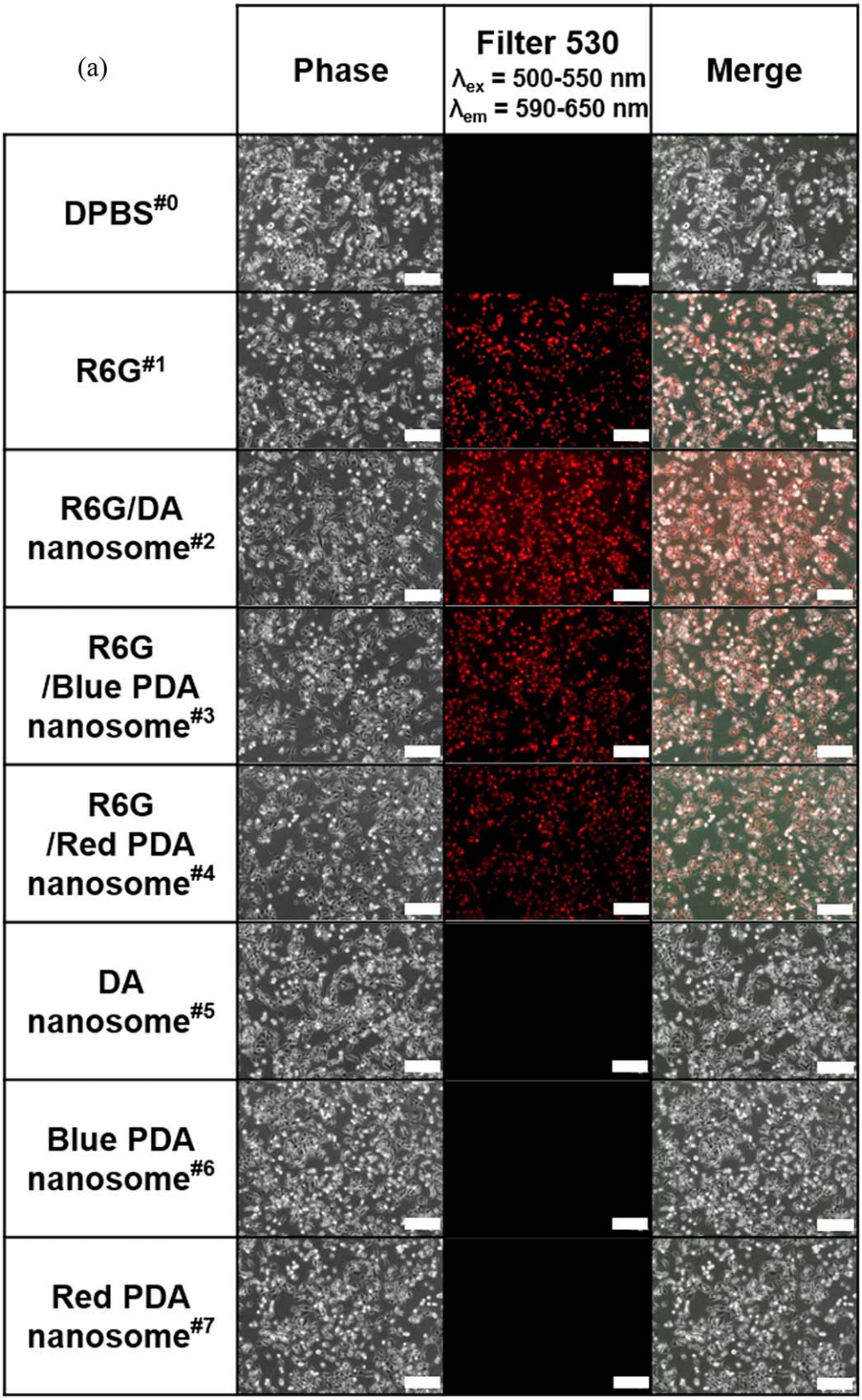

Figure 5. Fluorescence and confocal microscopy images of MDA-MB-231 cells after 24 h of treatment with the nanosomes (1/10 serial dilution of stock solutions of R6G (0.008 33 mM) or/and PCDA (0.5 mM)). Scale bars of the fluorescence, confocal, and magnified confocal images numbered 1–4 are 200 μm, 20 μm, and 10 μm, respectively. (a) Fluorescence images of MDA-MB-231 cells obtained using a 10×objective lens. Red fluorescence (R6G/Red PDA, λ_{ex} = 500–550 nm, λ_{em} = 590–650 nm). (b) Confocal microscopy images of MDA-MB-231 cells obtained using a 63×objective lens. Blue fluorescence (stained with endocytosis marker EEA1, λ_{ex} = 332 nm, λ_{em} = 435 nm); Red fluorescence (R6G/Red PDA, λ_{ex} = 497 nm, λ_{em} = 524 nm). *MIP = Maximum Intensity Projections.

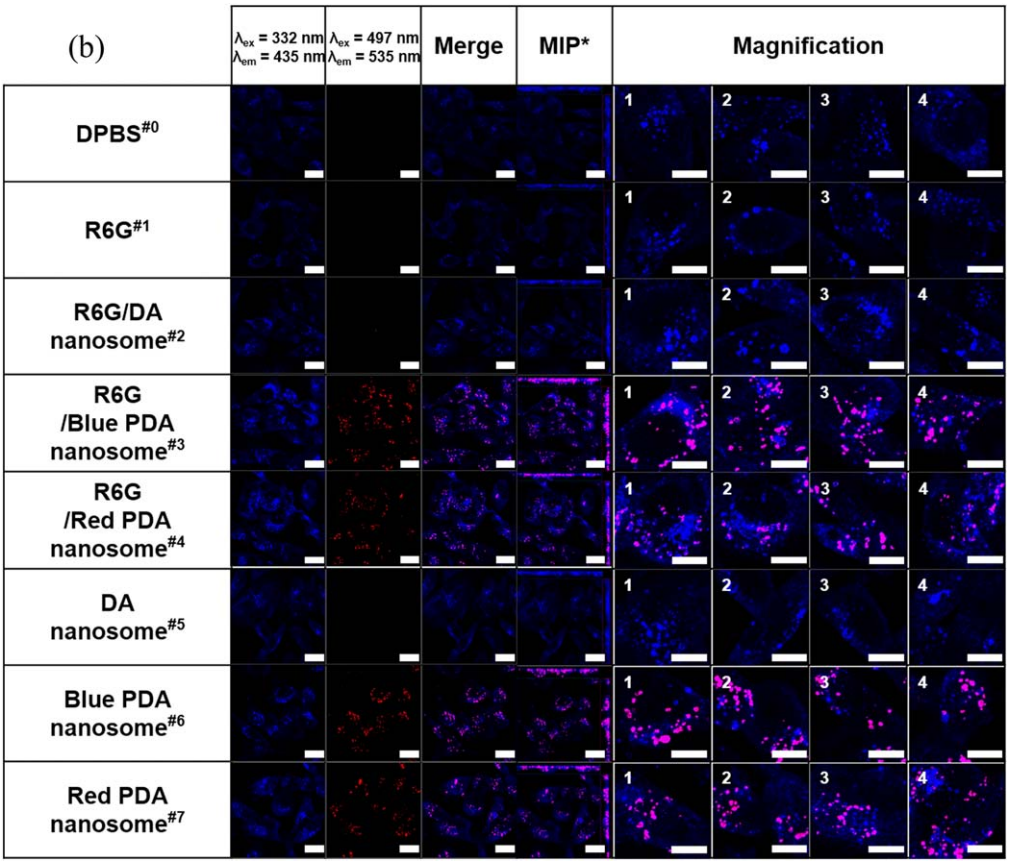

Figure 5. (Continued.)

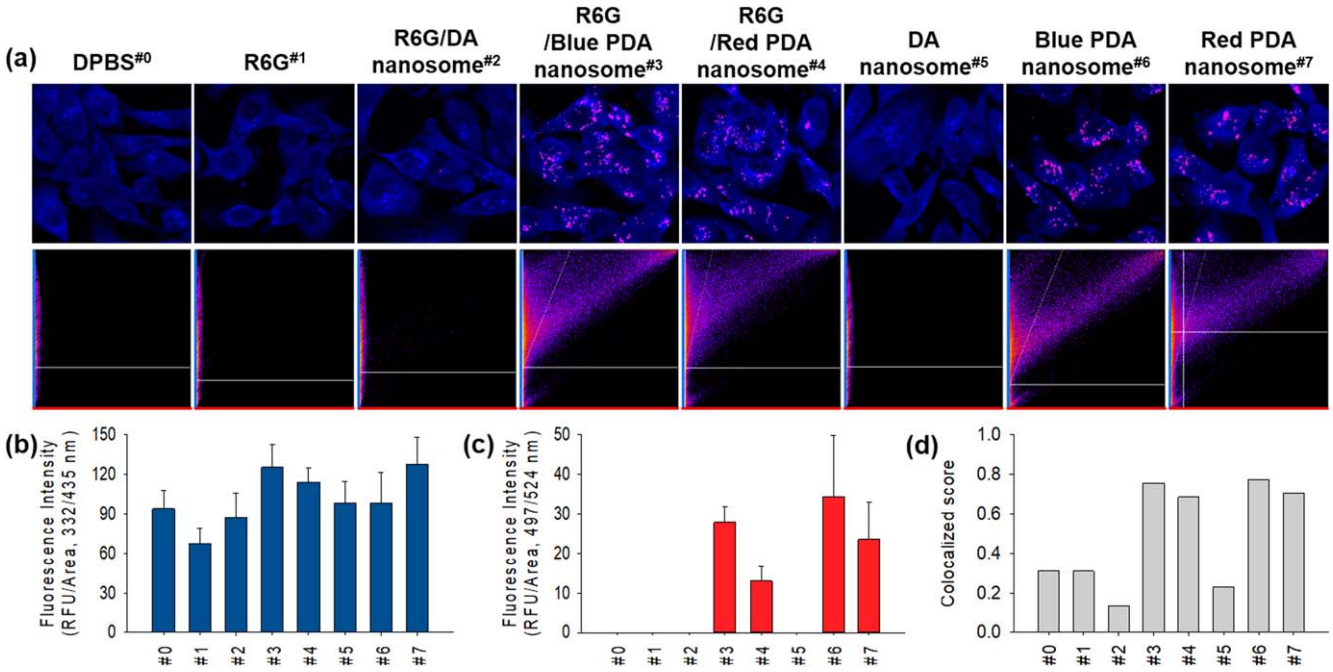

Figure 6. (a) Confocal microscopy images (upper column) and their colocalization plots (lower column, *x*-axis: red, *y*-axis: blue) of MDA-MB-231 cells after 24 h of treatment with the nanosomes. Blue fluorescence (stained with endocytosis marker EEA1, $\lambda_{ex} = 332$ nm, $\lambda_{em} = 435$ nm); Red fluorescence (R6G/Red PDA, $\lambda_{ex} = 497$ nm, $\lambda_{em} = 524$ nm). (b) Blue fluorescence intensity graph and (c) red fluorescence intensity graph from (a) upper column. (d) Colocalized score graph from (a) lower column.

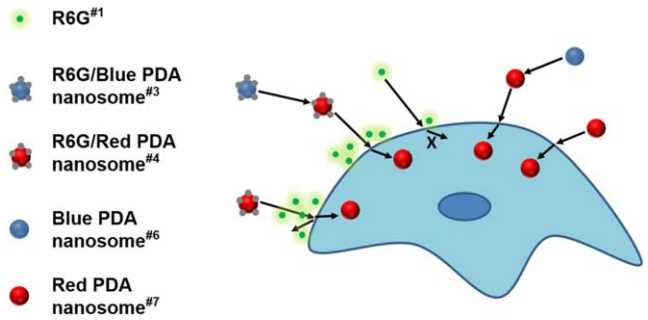

Figure 7. Proposed mechanism for cellular uptake of PDA-based nanosomes.

microscopic images using the ImageJ software. We added the relative fluorescence intensities of the red and blue color values and co-localized the pixel map with the relevant colocalized score in figure 6. In figure 6(b), the number of blue spots are shown to increase after the treatment of the nanosomes with and without R6G. The red spots from PDA nanosomes were detected from confocal microscopy (figure 6(c)). In figures 6(a) (lower column) and (c), colocalization between blue endosomes and red nanosomes are depicted and quantified. When the cells were treated with the PDA nanosomes, the nanosomes were internalized into the cells, and the colocalized scores increased due to the overlapping between the endosomes and nanosomes. However, red spots at the intracellular region were not observed without nanosome treatment. Based on these results, we believe that the red fluorescence of the R6G/Blue PDA nanosome (#3) and the R6G/Red PDA nanosome (#4) in FM images at filter 530 is due to R6G and not PDA. It suggests that R6G may dissociate near the cell surface due to a stronger electrostatic interaction between the cationic R6G and the anionic cell membrane. The quenching of R6G in the single platforms (R6G/Blue PDA nanosome, #3; R6G/Red PDA nanosome, #4) was observed in the FM spectra (figure 2(d)). R6G is 'switched on' when it dissociates [27], as observed in the FM images for #3 and #4. In addition, the CFM images of #3, #4, #6, and #7 showed intracellular red fluorescence, demonstrating the cellular uptake of dissociated PDA nanosomes (e.g. endocytosis). In the CFM images, blue fluorescent spots from EEA1 as an endocytosis marker was increased when treated with PDA-based nanosomes (#3, #4, #6, and #7). This kind of fluorescence enhancement in endosomal markers has been observed when nanoparticles penetrate into cells. Moreover, red fluorescent spots from PDA-based nanosomes co-localized with the endosomes as shown in figure 5(b)-magnification.

Current review articles described various internalization pathways of nanoparticles for development of nanomedicine [32–34]. One of the endocytosis mechanisms, non-ligand targeted our nanocarriers having electrostatic interaction between the R6G and PDA nanosome. This association or dissociation is straightforwardly influenced under high ionic strength [35–37]. In our previous study [27], de-quenching (or dissociation) of R6G dye from PDA nanosome was observed under a physiological environment by the charge screening effect. Based on the cell viability and endocytosis studies, when the R6G/Blue or Red nanosome are close to cell, the R6G would be dissociated or attracted to counter-ionic cell membrane, while the dissociated nanosome is internalized into cell (figure 7).

4. Conclusions

The effects of PDA-based nanosomes on cell viability and how they move toward cell environments were investigated. Nanosomes containing a higher degree of polymerization were found to be less toxic and should be considered when designing PDA-based nanocarriers for *in vitro* studies and further translational research. Moreover, the proposed novel mechanism of PDA-based nanosome internalization into cells provides important insights for developing systemic nanocarriers for drug/gene delivery, chemo/biosensing platforms, and imaging probes.

Acknowledgments

This work was supported by a National Research Foundation of Korea (NRF) grant funded by the Korea government (MSIP: Ministry of Science, ICT & Future Planning) (2017R1C1B5018327, 2017R1C1B2010867) and a grant of the Korea Health Technology R&D Project through the Korea Health Industry Development Institute (KHIDI), funded by the Ministry of Health & Welfare, Republic of Korea (HI17C2586).

Author contributions

Notes: The authors declare no competing financial interest.

ORCID iDs

Sungbaek Seo https://orcid.org/0000-0001-5813-4616

References

[1] Bobo D, Robinson K J, Islam J, Thurecht K J and Corrie S R 2016 *Pharm. Res.* **33** 2373
[2] Merino S, Martín C, Kostarelos K, Prato M and Vázquez E 2015 *ACS Nano* **9** 4686
[3] Yang K, Feng L and Liu Z 2016 *Adv. Drug. Deliv. Rev.* **105** 228
[4] Jiang Z, Le N D B, Gupta A and Rotello V M 2015 *Chem. Soc. Rev.* **44** 4264
[5] Bharti C, Gulati N, Nagaich U and Pal A 2015 *Int. J. Pharm. Invest.* **5** 124
[6] Jenkins R, Burdette M K and Foulger S H 2016 *RSC Adv.* **6** 65459
[7] Schäferling M 2016 *Wiley Interdiscip. Rev. Nanomedicine Nanobiotechnology* **8** 378
[8] Carpick R W, Sasaki D Y and Burns A R 2000 *Langmuir* **16** 1270

[9] Ryu S, Yoo I, Song S, Yoon B and Kim J-M 2009 *J. Am. Chem. Soc.* **131** 3800
[10] Cheng Q and Stevens R C 1998 *Langmuir* **14** 1974
[11] Jonas U, Shah K, Norvez S and Charych D H 1999 *J. Am. Chem. Soc.* **121** 4580
[12] Tomioka Y, Tanaka N and Imazeki S 1989 *Thin Solid Films* **179** 27
[13] Tashiro K, Nishimura H and Kobayashi M 1996 *Macromolecules* **29** 8188
[14] Lee J, Jun H and Kim J 2009 *Adv. Mater.* **21** 3674
[15] Lee J, Seo S and Kim J 2012 *Adv. Funct. Mater.* **22** 1632
[16] Seo S, Lee J, Choi E-J, Kim E-J, Song J-Y and Kim J 2013 *Macromol. Rapid Commun.* **34** 743
[17] Mackiewicz N, Gravel E, Garofalakis A, Ogier J, John J, Dupont D M, Gombert K, Tavitian B, Doris E and Ducongé F 2011 *Small* **7** 2786
[18] Yao D, Li S, Zhu X, Wu J and Tian H 2017 *Chem. Commun.* **53** 1233
[19] Gravel E, Ogier J, Arnauld T, Mackiewicz N, Ducongé F and Doris E 2012 *Chem. Eur. J.* **18** 400
[20] Zhou G, Wang F, Wang H, Kambam S, Chen X and Yoon J 2013 *ACS Appl. Mater. Interfaces* **5** 3275
[21] Park D-H, Heo J-M, Jeong W, Yoo Y H, Park B J and Kim J-M 2018 *ACS Appl. Mater. Interfaces* **10** 5014
[22] Jiang H, Hu X-Y, Schlesiger S, Li M, Zellermann E, Knauer S K and Schmuck C 2017 *Angew. Chemie Int. Ed.* **56** 14526
[23] Gravel E, Thézé B, Jacques I, Anilkumar P, Gombert K, Ducongé F and Doris E 2013 *Nanoscale* 5, 1955
[24] Jundt C, Klein G and Le Moigne J 1993 *Chem. Phys. Lett.* **203** 37
[25] Olmsted J and Strand M 1983 *J. Phys. Chem.* **87** 4790
[26] Park K H, Yang S Y, An B-S, Hwang D Y, Lee J H, Kim H S and Seo S 2019 *J. Nanosci. Nanotechnol.* **19** 3755
[27] Seo S, Kwon M S, Phillips A W, Seo D and Kim J 2015 *Chem. Commun* **51** 10229
[28] Li X, Matthews S and Kohli P 2008 *J. Phys. Chem* B **112** 13263
[29] Seo S, Kim D, Jang G, Kim D-M, Kim D W, Seo B-K, Lee K-W and Lee T S 2013 *React. Funct. Polym.* **73** 451
[30] Sansee A, Kamphan A, Traiphol R and Kielar F 2016 *Colloids Surf.* A **497** 362
[31] Ogier J, Arnauld T, Carrot G, Lhumeau A, Delbos J-M, Boursier C, Loreau O, Lefoulon F and Doris E 2010 *Org. Biomol. Chem.* **8** 3902
[32] Yameen B, Choi W, Vilos C, Swami A, Shi J and Farokhzad O C 2014 *J. Control. Release* **190** 485
[33] Zhao J and Stenzel M H 2018 *Polym. Chem.* **9** 259
[34] Deng J and Gao C 2016 *Nanotechnology* **27** 412002
[35] Gucht J, Spruijt E, Lemmers M and Stuart M A C 2011 *J. Colloid Interface Sci.* **361** 407
[36] Perry S L *et al Nat. Commun.* 2015 **6** 6052
[37] Wei W, Tan Y, Rodriguez N R M, Yu J, Israelachvili J N and Waite J H 2014 *Acta Biomater.* **10** 1663